Concentration-Dependent Near-Infrared to Visible Upconversion in Nanocrystalline and Bulk Y_2O_3:Er^{3+}

Fiorenzo Vetrone,[†] John-Christopher Boyer,[†] John A. Capobianco,*[,†] Adolfo Speghini,[‡] and Marco Bettinelli[‡]

Department of Chemistry and Biochemistry, Concordia University, 1455 de Maisonneuve Boulevard W, Montreal, Quebec, H3G-1M8, Canada, and Dipartimento Scientifico e Tecnologico, Università di Verona, and INSTM, UdR Verona, Ca' Vignal, Strada Le Grazie 15, I-37134 Verona, Italy

Received January 30, 2003. Revised Manuscript Received April 15, 2003

We investigated the upconversion properties of nanocrystalline and bulk Y_2O_3:Er^{3+} as a function of the erbium concentration (1, 2, 5, 10, 25, and 35 mol %). Following excitation with 980 nm, upconverted emission is observed from the $^2H_{11/2}$, $^4S_{3/2}$, and $^4F_{9/2}$ excited states to the $^4I_{15/2}$ ground state centered at 525, 550, and 660 nm, respectively. As the dopant concentration is increased, the upconverted luminescence revealed not only an overall increase in intensity but also an enhancement of the red ($^4F_{9/2} \rightarrow {}^4I_{15/2}$) emission with respect to the green ($^2H_{11/2}$, $^4S_{3/2} \rightarrow {}^4I_{15/2}$) emission. A cross-relaxation process is involved in populating the $^4F_{9/2}$ state, which bypasses the green-emitting states. Blue upconversion, observed in bulk Y_2O_3:Er^{3+} only, also showed a concentration dependence. The population of the $^2P_{3/2}$ state was achieved through a three-step phonon-assisted energy-transfer process.

Introduction

The search for novel light-emitting materials has been the subject of continuous study since the early part of the previous century. Recently, with the advent of new techniques allowing for the facile synthesis of nanosized phosphors, it has become possible to control both the size and shape of many of the most commonly used luminescent materials. These phosphors with particle dimensions in the nanometer regime have of late become the focus of intense study as the associated size restrictions and extraordinarily large surface areas incur changes in the spectroscopic properties of these materials.[1] As many electronic devices are being reduced in size, the development of phosphors with particle sizes in the nanometer regime has become vital. An excellent example is the development of flat panel displays where design constraints severely limit the amount of excitation power available for the excitation of phosphors.[2] Consequently, there is an ongoing search for luminescing materials with increased efficiency and smaller size.

The majority of the work has focused on semiconducting nanocrystals such as ZnS[3,4] and CdS.[5] However, there has also been a considerable amount of research on doped insulators, in particular, rare-earth-doped nanocrystalline materials. For the most part, the material of choice has been Y_2O_3,[6−8] but work has also been done on other sesquioxides, Lu_2O_3[9−11] and Gd_2O_3,[12] as well as some isostructural vanadates such as YVO_4 and $GdVO_4$.[13,14] Aside from its ease of synthesis in the nanometer regime, yttria possesses favorable physical properties such as a high melting point, phase stability, and low thermal expansion,[15] making it an excellent host material for rare earth ions.

The Er^{3+} ion can efficiently emit photons in the blue, green, and red regions of the spectrum and has the ability to convert infrared light to visible. This phenomenon whereby the material emits light that has higher photon energy than the pump source is known as upconversion and, for this reason, the Er^{3+} ion is widely used in upconversion phosphors and as an upconversion laser active ion. The tripositive erbium ion is an ideal candidate for upconversion since its electronic energy level scheme allows for many radiative transitions to

* To whom correspondence should be addressed. E-mail: capo@vax2.concordia.ca.

[†] Concordia University.

[‡] Università di Verona.

(1) Liu, G. K.; Zhuang, H. Z.; Chen, X. Y. *Nano Lett.* **2002**, *2*, 535−539.

(2) Tallant, D. R.; Seager, C. H.; Simpson, R. L. In *Materials Research Society Spring Meeting*; Jensen, K. L., Mackie, W., Temple, D., Itoh, J., Nemanich, R., Trottier, T., Holloway, P., Eds.; Materials Research Society: San Francisco, CA, 2000; Vol. 621.

(3) Bhargava, R. N.; Gallagher, D.; Hong, X.; Nurmikko, A. *Phys. Rev. Lett.* **1994**, *72*, 416−419.

(4) Bol, A. A.; Meijerink, A. *J. Lumin.* **2000**, *87*, 315−318.

(5) van Oijen, A. M.; Verberk, R.; Durand, Y.; Schmidt, J.; van Lingen, J. N. J.; Bol, A. A.; Meijerink, A. *Appl. Phys. Lett.* **2001**, *79*, 830−832.

(6) Tissue, B. M. *Chem. Mater.* **1998**, *10*, 2837−2845.

(7) Capobianco, J. A.; Vetrone, F.; D'Alesio, T.; Tessari, G.; Speghini, A.; Bettinelli, M. *Phys. Chem. Chem. Phys.* **2000**, *2*, 3203−3207.

(8) Capobianco, J. A.; Vetrone, F.; Boyer, J. C.; Speghini, A.; Bettinelli, M. *J. Phys. Chem. B* **2002**, *106*, 1181−1187.

(9) Capobianco, J. A.; Vetrone, F.; Boyer, J. C.; Speghini, A.; Bettinelli, M. *Opt. Mater.* **2002**, *19*, 259−268.

(10) Zych, E.; Hreniak, D.; Strek, W. *J. Phys. Chem. B* **2002**, *106*, 3805−3812.

(11) Zych, E. *J. Phys.: Condens. Matter* **2002**, *14*, 5637−5650.

(12) Soo, Y. L.; Huang, S. W.; Kao, Y. H.; Yang, Y. W.; Lai, L. J.; Chhabra, V.; Kulkarni, B.; Veliadis, J. V. D.; Bhargava, R. N. *Mod. Phys. Lett. B* **2001**, *15*, 205−211.

(13) Riwotzki, K.; Hasse, M. *J. Phys. Chem. B* **2001**, *105*, 12709−12713.

(14) Mahalley, B. N.; Pode, R. B.; Gupta, P. K. *Phys. Status Solidi A* **2000**, *177*, 293−302.

(15) Laversenne, L.; Kairouani, S.; Guyot, Y.; Goutaudier, C.; Boulon, G.; Cohen-Adad, M. T. *Opt. Mater.* **2002**, *19*, 59−66.

10.1021/cm0301930 CCC: $25.00
Published on Web 06/11/2003

occur. The excited states of the Er^{3+} ion possess long lifetimes and thus can be conveniently populated by the absorption of photons in the near-infrared (NIR) region.

The efficiency of Er^{3+} upconversion is governed by two principal factors: the rate of multiphonon relaxation, which depends on the phonon energies of the host and the concentration of dopant ions. In particular, in a lattice with low phonon energies, the decay of an excited level of a rare earth ion is predominantly radiative, due to inefficient multiphonon relaxation. Moreover, an excess of dopant ion concentration can also hinder the upconversion process due to cross-relaxation mechanisms. However, the extent depends mainly on the host material.

On the other hand, the current interest in upconversion is due also to the availability of low-cost NIR laser diodes, which could populate the Er^{3+} ion levels at 800 or 980 nm and give rise to intense visible light. To extend our previous investigation on the upconversion properties of nanocrystalline and bulk Y_2O_3:Er^{3+} by exciting at 800 nm,[8] we discuss in this paper the effects of varying the Er^{3+} ion concentration on the upconversion of nanocrystalline and bulk Y_2O_3:Er^{3+} by exciting at 980 nm.

Experimental Section

Sample Preparation. Nanocrystalline cubic Y_2O_3 samples doped with 1, 2, 5, and 10 mol % Er_2O_3 (of composition $Y_{1.98}Er_{0.02}O_3$, $Y_{1.96}Er_{0.04}O_3$, $Y_{1.90}Er_{0.10}O_3$, and $Y_{1.80}Er_{0.20}O_3$, respectively) were prepared using a solution combustion (propellant) synthesis procedure,[16,17] which involves the exothermic reaction between a metal nitrate (oxidizer) and an organic fuel, such as glycine. The stoichiometric synthesis reaction is

$$6M(NO_3)_3 + 10NH_2CH_2COOH + 18O_2 \rightarrow 3M_2O_3 + 5N_2 + 18NO_2 + 20CO_2 + 25H_2O$$

where M = Y, Er. The size of the nanopowders is greatly influenced by the reaction temperature and can be controlled by adjusting the glycine-to-metal nitrate molar ratio.[16] A molar ratio of 1.2:1 was employed to prepare the aqueous precursor solution, which according to the literature should allow the formation of small size yttria particles.[16]

A detailed investigation using wide-angle X-ray scattering (WAXS) was carried out to determine the average size of the Y_2O_3 crystallites obtained by propellant synthesis.[18] The WAXS patterns for the nanocrystalline material indicated that the crystalline domains preserve the crystallographic structure of yttria (cubic system; space group *Ia*3) and that the average radius of the crystallites was ≈20 nm.

For purposes of comparison, bulk samples doped with 1, 2, 5, 10, 25, and 35 mol % Er_2O_3 (of composition $Y_{1.98}Er_{0.02}O_3$, $Y_{1.96}Er_{0.04}O_3$, $Y_{1.90}Er_{0.10}O_3$, $Y_{1.80}Er_{0.20}O_3$, $Y_{1.50}Er_{0.50}O_3$, and $Y_{1.30}Er_{0.70}O_3$, respectively) were prepared by intimately mixing Y_2O_3 (Aldrich, 99.99%) and Er_2O_3 (Aldrich, 99.99+%), pressing the powders into pellets under 10 tons of pressure, and firing them in air at 1500 °C for 48 h. At this temperature, the optimum homogeneity (verified using scanning electron microscopy) was obtained.

All yttria samples were kept in air without any further precaution.

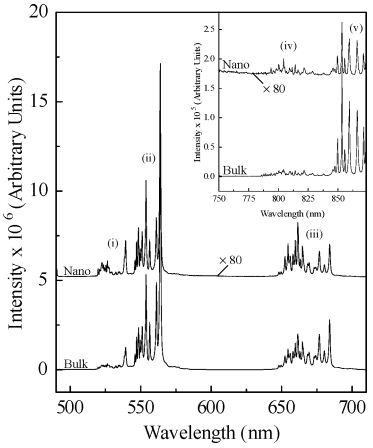

Figure 1. Room-temperature luminescence of nanocrystalline and bulk Y_2O_3:Er^{3+} (10 mol %) upon excitation at 488 nm. (i) $^2H_{11/2} \rightarrow {}^4I_{15/2}$; (ii) $^4S_{3/2} \rightarrow {}^4I_{15/2}$; (iii) $^4F_{9/2} \rightarrow {}^4I_{15/2}$. Inset: (iv) $^4I_{9/2} \rightarrow {}^4I_{15/2}$; (v) $^4S_{3/2} \rightarrow {}^4I_{13/2}$.

Reflectance Spectroscopy. The diffuse reflectance spectra in the medium infrared (MIR) region were measured at room temperature with a Nicolet Magna 760 FTIR spectrometer using an aluminated mirror as a reference.

Emission Spectroscopy. Luminescence spectra were measured by exciting either at 488 nm using a Coherent Sabre Innova, 20-W argon ion laser, or at 980 nm using a Spectra-Physics Model 3900 titanium sapphire laser pumped by the 514.5-nm line of a Coherent Sabre Innova argon ion laser. The visible emissions were then collected and dispersed using a Jarrell-Ash 1-m Czerny Turner double monochromator. The signals were monitored with a thermoelectrically cooled Hamamatsu R943-02 photomultiplier tube. The photomultiplier signals were processed by a preamplifier model SR440 Stanford Research Systems. A gated photon counter model SR400 Stanford Research Systems data acquisition system was used as an interface between the computer and the spectroscopic hardware. The signal was recorded under computer control using the Stanford Research Systems SR465 software data acquisition/analyzer system.

A continuous flow cryostat (Janis Research ST-VP-4) was used to acquire the low-temperature spectra and a Lakeshore model 330 controller was used to monitor the temperature.

The decay times were obtained by modulating the cw excitation sources mentioned above using an optical chopper (Stanford Research Systems, model SR 540) and were recorded using the gated photon counter. The temporal dependence of the upconverted emission was obtained by modulating the excitation beam at 20 Hz with the chopper and the photomultiplier tube output recorded using a digital oscilloscope (Tektronix TDS 520A).

Results and Discussion

The room-temperature emission spectra of Er^{3+}-doped nanocrystalline and bulk Y_2O_3, following excitation at 488 nm, were reported in a previous paper.[8] However, for illustrative purposes, Figure 1 presents the emission spectra (λ_{exc} = 488 nm) for the 10 mol % nanocrystalline and bulk samples in which we observe four transitions in the green, red, and NIR portions of the spectrum. The Y_2O_3 lattice crystallizes in a cubic bixbyite structure (space group *Ia*3)[19] and possesses two distinct crystallographic sites available for rare earth ion substitution:[20,21] one site with point group symmetry C_2 and the

(16) Tao, Y.; Zhao, G.; Zhang, W.; Xia, S. *Mater. Res. Bull.* **1997**, *32*, 501−506.

(17) Tessari, G.; Bettinelli, M.; Speghini, A.; Ajò, D.; Pozza, G.; Depero, L. E.; Allieri, B.; Sangaletti, L. *Appl. Surf. Sci.* **1999**, *144*−*145*, 686−689.

(18) Polizzi, S.; Fagherazzi, G.; Battagliarin, M.; Bettinelli, M.; Speghini, A. *J. Mater. Res.* **2001**, *16*, 146−154.

(19) Wyckoff, R. W. G. *Crystal Structures*, 2nd ed.; Interscience: New York, 1964; Vol. 2.

(20) Saiki, A.; Ishizawa, N.; Mizutani, N.; Kato, M. *J. Ceram. Soc. Jpn.* **1985**, *93*, 649−654.

other with C_{3i} symmetry. The latter C_{3i} site has an associated center of inversion and as such the selection rules dictate that all electric dipole transitions are forbidden. And thus, the 4f spectra presented in Figure 1 exhibit electric dipole transitions from the Er^{3+} ions residing in the C_2 sites and magnetic dipole transitions from both sites.

In all samples under investigation, green emission was observed and attributed to the transition from the $^2H_{11/2}$ and $^4S_{3/2}$ states to the $^4I_{15/2}$ ground state, centered at 525 and 550 nm, respectively. Red emission was observed centered at 660 nm, attributed to the transition from the $^4F_{9/2}$ level to the ground state. Also, relatively weak NIR emission was observed centered at 810 and 860 nm, respectively, and is ascribed to the $^4I_{9/2} \rightarrow {}^4I_{15/2}$ and $^4S_{3/2} \rightarrow {}^4I_{13/2}$ transitions.

The same experiment performed at low temperature (77 K) showed spectral features to the room-temperature data. However, these spectra differ in that the $^2H_{11/2} \rightarrow {}^4I_{15/2}$ transition was not observed in the nanocrystalline and bulk samples at 77 K. In a previous paper,[22] we showed that the $^4S_{3/2}$ level is responsible for thermally populating the $^2H_{11/2}$ state, which lies $\approx$700 cm^{-1} higher in energy. At low temperatures, the feeding of the $^2H_{11/2}$ state from the $^4S_{3/2}$ state is very low and thus the intensity of the $^4S_{3/2} \rightarrow {}^4I_{15/2}$ transition increases with respect to the $^2H_{11/2} \rightarrow {}^4I_{15/2}$ one. As the temperature is raised, the $^2H_{11/2}$ level is populated thermally at the expense of the $^4S_{3/2}$ level, causing the intensity of the $^2H_{11/2} \rightarrow {}^4I_{15/2}$ transition to increase while the intensity of the $^4S_{3/2} \rightarrow {}^4I_{15/2}$ transition decreases proportionally.

Also of note is the fact that the 77 K emission spectrum of nanocrystalline $Y_2O_3:Er^{3+}$ is broadened compared to that of the identically doped bulk counterpart. An explanation for this phenomenon was recently presented by Liu et al.[1] In nanocrystalline materials, the influence of defects in the host lattice as well as contamination on their surface cannot be ignored and they induce inhomogeneous broadening not unlike what occurs in rare-earth-doped glasses. In fact, with the size restrictions associated with the nanocrystalline material, a greater fraction of the rare earth ions will lie on the surface compared to the bulk material. Those ions on the surface of the particle should have a more disordered environment with respect to the ions in the particle center (in the C_2 and C_{3i} sites). Without any type of selective excitation, the spectra of nanocrystalline $Y_2O_3:Er^{3+}$ will consist of emissions from both types of Er^{3+} ions. The surface ions would give rise to a broader emission profile and thus the luminescence spectrum of the doped nanopowders would be more inhomogeneously broadened compared with the emission spectrum of the Er^{3+}-doped bulk material.

In nanocrystalline yttrium oxide, CO_2 and H_2O are produced as byproducts of the propellant synthesis reaction and could be adsorbed immediately after the formation of the nanoparticles. As the preparation is performed in air, CO_2 and H_2O could be adsorbed from air as well. The residual nitrate ions are decomposed after firing the nanocrystals at 500 °C for 1 h, as was evidenced by the absence of their characteristic bands in the MIR and Raman spectra. However, this heat treatment was not sufficient enough to remove either the carbonate or the hydroxyl ions from the surface of the nanopowders. The MIR spectra obtained after the heat treatment show bands occurring at ca. 1500 and 3350 cm^{-1} and are assigned to vibrations from the carbonate and hydroxyl groups, respectively (see Figure 2). To reduce the amount of CO_3^{2-} and OH^- ions on the surface of the nanoparticles, additional heat treatments on a nanocrystalline $Y_{1.80}Er_{0.20}O_3$ sample were carried out. Initially, the sample was treated at 800 °C for 17 h and subsequently cooled to room temperature. The same sample was further treated at 1000 °C for 65 h and then cooled again to room temperature. From the MIR spectra of the doped nanoparticles after the successive heat treatments, bands were still observed at ca. 1500 and 3350 cm^{-1} (Figure 2). After the second heat treatment, the overall intensities of the bands at 1500 and 3350 cm^{-1} indicate that the heat treatments did reduce the overall surface contamination but, in the present experimental conditions, the contaminants were not completely removed (Figure 2). On the other hand, a longer heat treatment at higher temperatures could induce an aggregation of the nanoparticles, a process in which they combine to form larger particles. In this case, as the spectroscopy of the nanocrystalline material is particle-size-dependent, a comparison between the luminescence of the heat-treated and non-heat-treated nanocrystalline materials could be difficult to make. We further undertook another thermal treatment on a nanocrystalline $Y_{1.98}Er_{0.02}O_3$ sample in which the nanocrystals were heated under a N_2 flow (2 L/min) for 2 h at 700 °C. The nanocrystals were then cooled to 200 °C under the N_2 flux, after which the sample was sealed in a vacuum box. Once the sample had cooled to room temperature, the MIR spectrum was immediately measured. Bands attributed to CO_2 and H_2O are still evidenced (Figure 2, inset). In Figure 2 a bulk sample is also shown for comparison and shows no bands at either 1500 or 3350 cm^{-1}, indicating the lack of adsorption of CO_2 and H_2O. Therefore, it is important to note

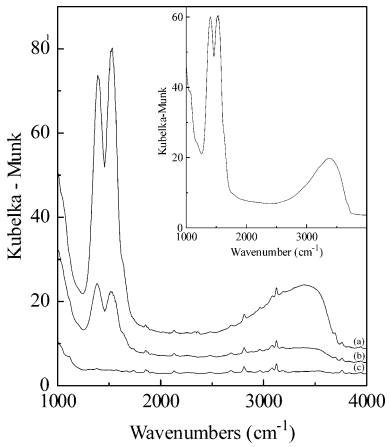

Figure 2. Diffuse reflectance spectra of nanocrystalline $Y_{1.80}Er_{0.20}O_3$ following sequential heat treatment: (a) 800 °C for 17 h; (b) 1000 °C for 65 h; (c) bulk $Y_{1.8}Er_{0.2}O_3$ sample shown for comparison. Inset: Diffuse reflectance spectrum of nanocrystalline $Y_{1.98}Er_{0.02}O_3$ following heat treatment under an N_2 flow (2 L/min) for 2 h at 700 °C.

(21) Xu, Y.-N.; Gu, Z.-q.; Ching, W. Y. *Phys. Rev. B* **1997**, *56*, 14993−15000.
(22) Vetrone, F.; Boyer, J. C.; Capobianco, J. A.; Speghini, A.; Bettinelli, M. *J. Phys. Chem. B* **2002**, *106*, 5622−5628.

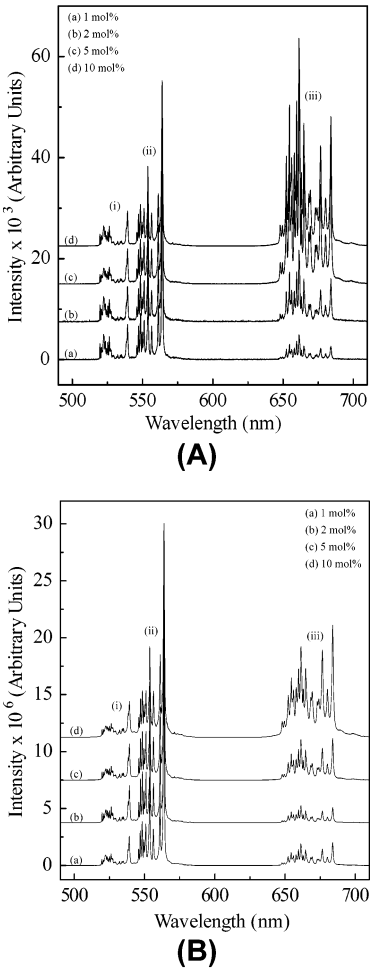

Figure 3. (A) Room-temperature luminescence of nanocrystalline Y_2O_3:Er^{3+} upon excitation at 980 nm. (i) $^2H_{11/2} \rightarrow {}^4I_{15/2}$; (ii) $^4S_{3/2} \rightarrow {}^4I_{15/2}$; (iii) $^4F_{9/2} \rightarrow {}^4I_{15/2}$. (B) Room-temperature luminescence of bulk Y_2O_3:Er^{3+} upon excitation at 980 nm. (i) $^2H_{11/2} \rightarrow {}^4I_{15/2}$; (ii) $^4S_{3/2} \rightarrow {}^4I_{15/2}$; (iii) $^4F_{9/2} \rightarrow {}^4I_{15/2}$.

that when the optical properties of nanocrystalline Y_2O_3:Er^{3+} or related materials obtained by the same synthesis technique are being studied, the surface contaminants must be taken into account.

Excitation of nanocrystalline and bulk Y_2O_3:Er^{3+} with NIR radiation into the $^4I_{11/2} \leftarrow {}^4I_{15/2}$ absorption band (λ_{exc} = 980 nm) produced upconversion luminescence (Figures 3 and 4). Blue upconversion was observed with bands centered at 460, 475, and 495 nm, which are assigned to the $^4F_{5/2} \rightarrow {}^4I_{15/2}$, $^2P_{3/2} \rightarrow {}^4I_{11/2}$, and $^4F_{7/2} \rightarrow {}^4I_{15/2}$ transitions, respectively. The observed bands in the green region centered at 525 and 550 nm are assigned to the $^2H_{11/2} \rightarrow {}^4I_{15/2}$ and $^4S_{3/2} \rightarrow {}^4I_{15/2}$ transitions, respectively. Bands in the red region, centered at 660 nm, are assigned to the $^4F_{9/2} \rightarrow {}^4I_{15/2}$ transition. It should be noted that no blue upconversion was observed in the nanocrystalline samples.

The spectral band shapes and position are very similar to those obtained upon 488 nm excitation (see Figures 1 and 3). However, we observe a marked decrease in the overall luminescence intensity for the nanocrystalline material compared to its bulk counterpart. Clearly, the presence of adsorbed surface contaminants, such as CO_3^{2-} and OH^-, can be responsible for this decrease in upconversion luminescence. The nanocrystalline samples have available phonons of high

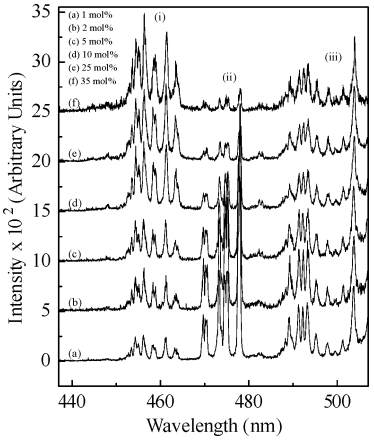

Figure 4. Upconverted emission of bulk Y_2O_3:Er^{3+} at room temperature, showing (i) $^4F_{5/2} \rightarrow {}^4I_{15/2}$, (ii) $^2P_{3/2} \rightarrow {}^4I_{11/2}$, and (iii) $^4F_{7/2} \rightarrow {}^4I_{15/2}$ (λ_{exc} = 980 nm).

Table 1. Room-Temperature Decay Time Constants (τ_m) for Nanocrystalline Y_2O_3:Er^{3+} Following Excitation with 980 nm

	decay times (μs)			
transition	1 mol %	2 mol %	5 mol %	10 mol %
$^4S_{3/2} \rightarrow {}^4I_{15/2}$	177	156	115	80
$^4F_{9/2} \rightarrow {}^4I_{15/2}$	280	262	215	163

wavenumbers, ~1500 cm^{-1}, due to the carbonate ions and ~3350 cm^{-1}, due to hydroxyl ions, compared to the bulk yttria material, for which the maximum phonon is about 600 cm^{-1}.[23,24] Therefore, the presence of these large vibrational quanta makes multiphonon relaxation in the nanocrystalline material much more efficient.

Table 1 shows the decay times of the green ($^4S_{3/2}$) and red ($^4F_{9/2}$) excited states in nanocrystalline Y_2O_3:Er^{3+} following excitation with 980 nm. The upconverted decay curves for all samples under investigation deviated slightly from single exponentiality. The same behavior was observed in Y_2O_3:Ho^{3+} nanocrystals[25] and was explained as being due to a distribution of dopant ions within the individual nanocrystals that were coupled in various degrees to the adsorbed surface molecules. The dopant ions located close to the particle surface would have a faster decay than those ions located inside the nanocrystals. In the nanocrystal material, a significant portion of the rare earth ions are located on the particle surface due to their small size and therefore lead to a nonexponential decay curve. Moreover, the presence of the adsorbed surface molecules on the nanocrystals were also responsible for the drastic difference between the decay times of the bulk and nanocrystal materials.[7] Furthermore, energy-transfer processes could also contribute in making the decay curves nonexponential. The emission decay time constants, τ_m, of nanocrystalline Y_2O_3:Er^{3+} were determined using the following equation,[26]

$$\tau_m = \frac{\int_0^\infty t\phi(t)\,dt}{\int_0^\infty \phi(t)\,dt} \quad (1)$$

where $\phi(t)$ is the intensity at time t. As seen from Table

(23) Weber, M. J. *Phys. Rev.* **1968**, *171*, 283−291.
(24) Riseberg, L. A.; Moos, H. W. *Phys. Rev.* **1968**, *174*, 429−438.

1, the decay times for the more heavily doped samples are considerably shorter in comparison to those that are more weakly doped and are caused by an increase in the interaction between Er^{3+} dopant ions.

The rise time of the temporal evolution of the green upconverted luminescence (not shown), due to the ($^2H_{11/2}$, $^4S_{3/2} \rightarrow {}^4I_{15/2}$) transition, is in excellent agreement with the lifetime of the $^4I_{11/2}$ level. From this behavior it is clearly evident that the $^4I_{11/2}$ level is the intermediate state in the upconversion process and, thus, acts as a population reservoir. The observed rate of depopulation (W) of the $^4I_{11/2}$ excited state is expressed as the sum of the radiative transition probability (W_R) and the nonradiative or multiphonon transition probability (W_{MPR}).[24] The radiative decay rates for the Er^{3+} ions in the bulk and nanocrystalline samples should reasonably be of the same order of magnitude; thus, the higher multiphonon transition probability in the nanopowders leads to lower upconversion luminescence intensity. The gap between the $^4I_{11/2}$ state and the next lower level, $^4I_{13/2}$, is $\approx$3600 cm^{-1}. Moreover, the energy gap between the thermalized ($^2H_{11/2}$, $^4S_{3/2}$) emitting levels and the next lower level, $^4F_{9/2}$, is about 3100 cm^{-1}, while the gap between the $^4F_{9/2}$ emitting level and the next lower level, $^4I_{9/2}$, is $\approx$2800 cm^{-1}. Therefore, the presence of the adsorbants on the nanocrystalline surface leads to a more efficient depopulation not only of the intermediate $^4I_{11/2}$ level but also of the emitting levels with respect to the bulk material. Consequently, lower upconversion luminescence intensity in the nanocrystalline material is expected, in agreement with the experimental results. From these considerations, it is no surprise that blue upconversion is not observed for the nanocrystalline samples but only for the bulk ones (see below).

As described above, $Y_2O_3:Er^{3+}$ (10 mol %) nanocrystals were heated at 800 °C for 17 h and subsequently at 1000 °C for 65 h. Once cooled to room temperature, the nanocrystalline sample was immediately sealed in a glass capillary and the upconversion luminescence (λ_{exc} = 980 nm) was measured. The upconversion spectrum of the heat-treated nanocrystalline sample, which was obtained under identical experimental conditions as the non-heat-treated sample, showed a small improvement in the luminescence intensity, but was still of much weaker intensity than the bulk sample. As we showed above, the heat treatments did not entirely remove the adsorbed H_2O and CO_2 from the surface of the nanocrystals. Therefore, the multiphonon relaxation rate is still greater than that in the bulk sample, having identical Er^{3+} concentration and resulting in observed weaker upconversion intensity.

A pronounced concentration dependence of the upconverted emission signal was observed for both the nanocrystalline and bulk material (see Figures 3 and 4). In the 1 mol % $Y_2O_3:Er^{3+}$ samples, the green ($^2H_{11/2}$, $^4S_{3/2} \rightarrow {}^4I_{15/2}$) emission dominates the spectrum following excitation at 980 nm. However, as the concentration of Er^{3+} is increased, we observe an enhancement of the red ($^4F_{9/2} \rightarrow {}^4I_{15/2}$) emission, which increases at a more rapid rate than the green emission. This effect is most striking in the nanocrystalline material, where in the 10 mol % sample, the red emission dominates over the green emission. A marked concentration dependence of the blue upconversion was also evidenced in bulk $Y_2O_3:Er^{3+}$. In the 1 mol % sample, the $^2P_{3/2} \rightarrow {}^4I_{11/2}$ transition dominates the spectrum in the 440−510-nm range. However, as the Er^{3+} ion concentration is increased, the intensity of the $^4F_{5/2} \rightarrow {}^4I_{15/2}$ transition increases, while the intensities of the $^2P_{3/2} \rightarrow {}^4I_{11/2}$ and $^4F_{7/2} \rightarrow {}^4I_{15/2}$ transitions decrease for the bulk samples.

To better comprehend the mechanism(s) which populate the ($^2H_{11/2}$, $^4S_{3/2}$) green- and ($^4F_{9/2}$) red-emitting levels, the upconversion luminescence intensity was measured as a function of the pump power. The slope of the curve of ln(Intensity) versus ln(Power) is $\approx$2 for both the green and red manifolds and for all samples under investigation. Therefore, the upconversion occurs via a two-photon process and can take place via three well-known mechanisms:[27−29] (i) excited state absorption (ESA); (ii) energy-transfer upconversion (ETU); and (iii) photon avalanche (PA). We can immediately rule out PA as a mechanism of upconversion in $Y_2O_3:Er^{3+}$ as no inflection point was observed in the power study.[30] So upconversion can occur either via ESA or ETU (Figure 5A). The mechanism for ESA is quite simple, as there exists an energy level which can be populated by absorption of a second 980-nm wavelength photon from the intermediate $^4I_{11/2}$ state. So the ion is excited to the $^4I_{11/2}$ intermediate state via a photon from the pump beam. Another photon in turn excites the same ion to the $^4F_{7/2}$ state. Nonradiative multiphonon decay is then responsible for populating the $^2H_{11/2}$, $^4S_{3/2}$, and $^4F_{9/2}$ states. Similarly, ETU can also populate the $^2H_{11/2}$, $^4S_{3/2}$, and $^4F_{9/2}$ states. In this mechanism, two Er^{3+} ions in close proximity are each excited to the $^4I_{11/2}$ state. One ion in turn transfers its energy to the other and nonradiatively decays back to the ground state. Consequently, the other ion is promoted to the $^4F_{7/2}$ state. ESA would be the most likely mechanism in samples with low dopant concentration as the dopant ions are too far apart to interact with each other. However, as the dopant concentration is increased, the probability of ETU occurring also increases. Evidence of ETU is provided by the upconverted decay times (λ_{exc} = 980 nm), which are lengthened compared to those obtained following direct excitation of the $^4F_{7/2}$ excited state with 488 nm.[7] Lengthening of the upconverted decay times alludes to the presence of energy transfer in the upconversion process.

If the above mechanisms were solely responsible for the upconversion, we would then expect upconversion spectra (λ_{exc} = 980 nm) that have identical relative intensities of the green and red transitions as the direct excitation (λ_{exc} = 488 nm) spectra. This clearly is not the case as we observe an enhancement of the red emission as the Er^{3+} concentration is increased. Thus, we propose that another mechanism is responsible for populating the $^4F_{9/2}$ state only. A mechanism for the direct two photon population of the $^4F_{9/2}$ state is ruled

(25) Capobianco, J. A.; Boyer, J. C.; Vetrone, F.; Speghini, A.; Bettinelli, M. *Chem. Mater.* **2002**, *14*, 2915−2921.
(26) Nakazawa, E. In *Phosphor Handbook*; Shionoya, S., Yen, W. M., Eds.; CRC Press: Boca Raton, FL, 1999.
(27) Bloembergen, N. *Phys. Rev. Lett.* **1959**, *2*, 84−85.
(28) Auzel, F. *C. R. Acad. Sci. (Paris)* **1966**, *262*, 1016−1019.
(29) Chivian, J. S.; Case, W. E.; Eden, D. D. *Appl. Phys. Lett.* **1979**, *35*, 124−125.
(30) Joubert, M. F.; Guy, S.; Jacquier, B. *Phys. Rev. B* **1993**, *48*, 10031−10037.

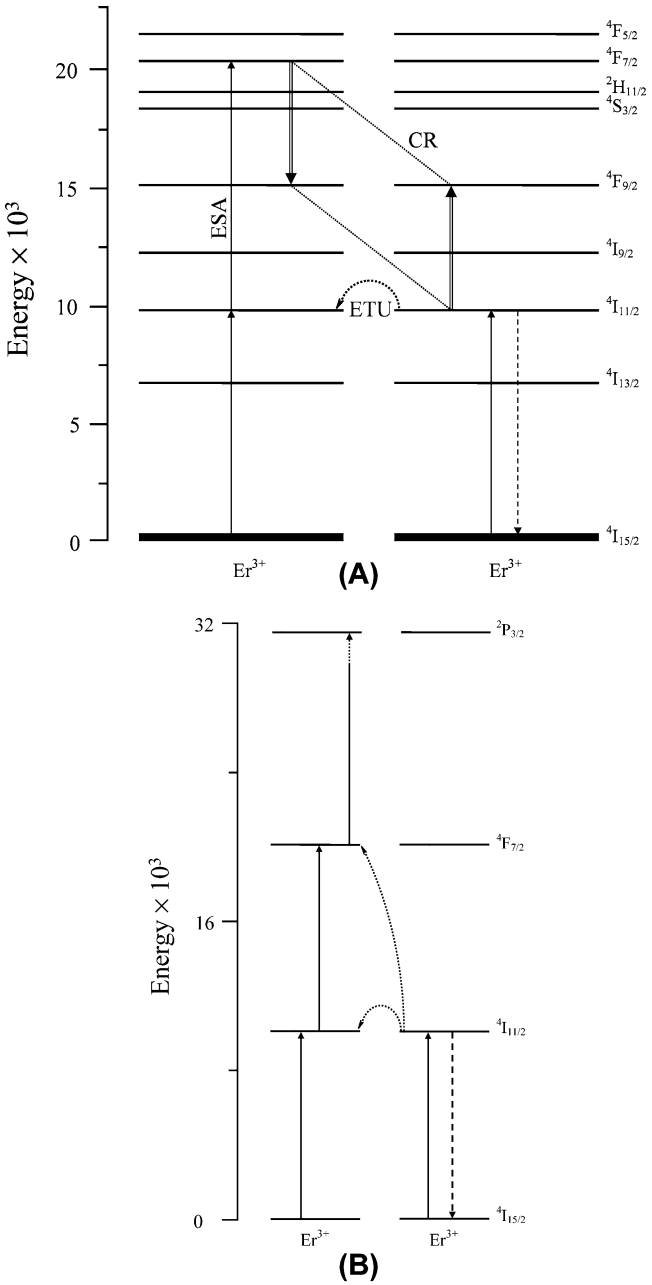

Figure 5. (A) Schematic representation of the excited-state absorption (ESA) and energy-transfer upconversion (ETU) mechanisms. The $^4F_{7/2} \rightarrow {}^4F_{9/2}$ and $^4F_{9/2} \leftarrow {}^4I_{11/2}$ cross-relaxation (CR) process responsible for populating the $^4F_{9/2}$ state is also shown. (B) Schematic representation of the three-step phonon-assisted energy-transfer (PET) upconversion process responsible for populating the $^2P_{3/2}$ state.

out as no resonance exists; therefore, there must exist some process that allows for the bypassing of the $^2H_{11/2}$ and $^4S_{3/2}$ levels and transferring of the pump energy to the $^4F_{9/2}$ state. We propose that a cross-relaxation process is responsible for populating the $^4F_{9/2}$ level and occurs via two resonant transitions (Figure 5A): $^4F_{7/2} \rightarrow {}^4F_{9/2}$ and $^4F_{9/2} \leftarrow {}^4I_{11/2}$.[31] In fact, the efficiency of the cross-relaxation process would increase on decreasing the average distance between the dopant ions and therefore with increasing the Er^{3+} concentration, giving rise to the enhancement of the red emission, in agreement with the obtained experimental data (see Figure 3).

We have discussed the mechanisms responsible for populating the $^2H_{11/2}$, $^4S_{3/2}$, and $^4F_{9/2}$ states. However, we cannot rule out the presence of even more upconversion mechanisms. We observe emission from the $^2P_{3/2}$ and $^4F_{5/2}$ states for the bulk yttria samples (see Figure 4), which is higher in energy than that in the $^4F_{7/2}$ state, which is populated by the ESA and ETU mechanisms. Therefore, it follows that other mechanism(s) may be operative beyond those previously discussed. This hypothesis was elucidated by the power study of the three manifolds in the blue region of the spectrum. This study revealed that the intensities of the $^4F_{5/2} \rightarrow {}^4I_{15/2}$ and $^4F_{7/2} \rightarrow {}^4I_{15/2}$ transitions obey a quadratic dependence while the intensity of the $^2P_{3/2} \rightarrow {}^4I_{11/2}$ transition obeys a cubic dependence on the pump power. That is, the $^4F_{5/2}$ and $^4F_{7/2}$ levels are populated via a two photon upconversion process, while three photon upconversion populates the $^2P_{3/2}$ state.

Again, as the relative intensities of the $^4F_{5/2} \rightarrow {}^4I_{15/2}$, $^2P_{3/2} \rightarrow {}^4I_{11/2}$, and $^4F_{7/2} \rightarrow {}^4I_{15/2}$ transitions change with the dopant concentration, we can presume that a concentration-dependent upconversion process is active. The mechanism to populate the $^4F_{7/2}$ state is described above. However, the $^4F_{5/2}$ level lies $\approx$1400 cm^{-1} higher in energy with respect to the $^4F_{7/2}$ level and thus two 980 nm wavelength photons do not have the necessary energy to populate the $^4F_{5/2}$ level. Therefore, it is conceivable that 2−3 intrinsic phonons of yttria can bridge the gap and allow for the population of the state via a phonon-assisted energy-transfer process (PET). The population of the $^2P_{3/2}$ level involves 3 photons, however; the Er^{3+} energy level diagram reveals that there is no energy level, which could be populated by a sequential absorption of three pump photons. In fact, if the $^4F_{7/2}$ level is populated by ESA or ETU, and nonradiatively decays to lower lying levels, again there is no energy level that could be populated by the absorption of another 980 nm wavelength pump photon. Similarly, if the ion in the ground state is excited by one photon to the $^4I_{11/2}$ level and then nonradiatively decays to the lower $^4I_{13/2}$ level, there is no higher energy state, which is resonant with the $^4I_{13/2}$ state. Therefore, we propose that another PET mechanism populates the $^2P_{3/2}$ level (Figure 5B) in which 1−2 phonons are requested to compensate the mismatch in energy ($\approx$690 cm^{-1}).

A possible explanation for the change in the relative intensities of the blue upconversion is the following. As shown in Figure 4, the intensity of the $^4F_{5/2} \rightarrow {}^4I_{15/2}$ transition increases significantly with increasing Er^{3+} concentration and this behavior is most probably due to the increasing number of emitting ions. On the other hand, the intensities of the $^2P_{3/2} \rightarrow {}^4I_{11/2}$ and $^4F_{7/2} \rightarrow {}^4I_{15/2}$ transitions decrease as the concentration of Er^{3+} in the material increases. In particular, the $^2P_{3/2} \rightarrow {}^4I_{11/2}$ emission intensity almost disappears at the higher Er^{3+} concentration, indicating a dramatic decrease in the population of the $^2P_{3/2}$ state. An explanation for these behaviors could be invoked by considering that the efficiency of the ($^4F_{7/2}$, $^4I_{11/2} \rightarrow {}^4F_{9/2}$,$^4F_{9/2}$) cross-relaxation process, which depopulates the $^4F_{7/2}$ state, increases with increasing dopant concentration. Correspondingly,

(31) Wittke, J. P.; Ladany, I.; Yocom, P. N. *J. Appl. Phys.* **1972**, *43*, 595−600.

the intensity of the $^4F_{7/2} \rightarrow {}^4I_{15/2}$ emission would decrease, in agreement with the experimental data (see Figure 4). Moreover, since the $^2P_{3/2}$ level is populated starting from the $^4F_{7/2}$ level, a decrease in the population of the $^4F_{7/2}$ state would also translate into a decrease of the population of the $^2P_{3/2}$ state and therefore in a decrease of the intensity of the $^2P_{3/2} \rightarrow {}^4I_{11/2}$ emission, in agreement with our experimental findings.

Conclusions

The concentration dependence of the upconversion properties for nanocrystalline and bulk $Y_2O_3:Er^{3+}$ was studied. Following excitation at 980 nm, the green ($^2H_{11/2}$, $^4S_{3/2} \rightarrow {}^4I_{15/2}$) emission dominates the upconversion spectrum for both the 1 mol % doped nanocrystalline and bulk samples. However, as the concentration of Er^{3+} dopant is increased, an enhancement of the red ($^4F_{9/2} \rightarrow {}^4I_{15/2}$) emission was observed for both the doped nanocrystalline and bulk samples. This behavior was more pronounced in the nanocrystalline material where the red emission becomes more intense than the green one and occurs via a cross-relaxation mechanism, which bypasses the green-emitting levels, and populates the $^4F_{9/2}$ state. A concentration dependence of the blue $^4F_{5/2} \rightarrow {}^4I_{15/2}$, $^4P_{3/2} \rightarrow {}^4I_{11/2}$, and $^4F_{7/2} \rightarrow {}^4I_{15/2}$ upconverted emission was observed in the bulk material. The intensity of the $^4F_{5/2} \rightarrow {}^4I_{15/2}$ transition increases as a function of concentration while that of the $^4P_{3/2} \rightarrow {}^4I_{11/2}$ and $^4F_{7/2} \rightarrow {}^4I_{15/2}$ transitions decrease with increasing Er^{3+} content. Competition with the ($^4F_{7/2}$, $^4I_{11/2} \rightarrow {}^4F_{9/2}$, $^4F_{9/2}$) cross-relaxation process reduces the population in the $^4F_{7/2}$ state, and consequently in the $^2P_{3/2}$ state, resulting in lower upconverted intensities.

Acknowledgment. The authors gratefully acknowledge the Natural Science and Engineering Research Council of Canada and MURST (Project 9903222581_005) of Italy for financial support. The authors gratefully thank Erica Viviani (Università di Verona) for expert technical assistance.

CM0301930